DOI: 10.61782/fa.2023.0424

forum acusticum 2023

AEROACOUSTIC INTERACTION EFFECTS BETWEEN PARALLEL LOW-PRESSURE AXIAL FLOW FANS

Michail Vourakis[1*] **Mikael Karlsson**[2]
[1] Department of Mechanics and Maritime sciences, Chalmers University of Technology, Sweden
[2] Department of Engineering Mechanics, KTH Royal Institute of Technology, Sweden

ABSTRACT

Engineering applications involving multi-fan arrangements in close proximity face challenges including sound wave interference and inlet flow interactions. The former leading to beating effects and the latter to non-ideal inlet conditions, potentially affecting the aerodynamic and acoustic performance of the system. The herein study investigates the above within the application space of automotive cooling fans. Two identical low-pressure axial flow cooling fans, with rotating rings, were installed in parallel. Different inlet shroud lengths and spacing between the two fans' rotating centers were tested. Acoustic measurements were performed in a bespoke fan test rig, leading to sound power estimation along with acoustic beating investigation. Complementary velocity measurements upstream of the fan were performed using laser Doppler anemometry. This led to the identification of possible inlet flow interactions and upstream disturbances which match the acoustic spectra. Moreover, a single fan arrangement was documented as means of reference for the parallel fan system.

Keywords: *aeroacoustics, axial fan, acoustic interference, inlet flow interaction, parallel fans.*

1. INTRODUCTION

Installations with multiple parallel fans/propellers, can be utilized for volume flow/thrust increase, while extending the range of the system's operational envelope. The application spectrum is wide, including but not limited to small sized cooling fans for portable electronics, drones' propulsion system and cooling fan modules used in vehicles and mining. Having a geometrically compact parallel multi-fan arrangement is a requirement for many of these applications. Satisfying this requirement may lead to installations where fans are exposed to non ideal inlet flow profiles as well as inlet flow interaction phenomena between the fans. Subsequently this may alter the designed aerodynamic and acoustic performance. In the case of axial flow fans it is known that non ideal inlet conditions, including steady distortions and turbulence ingestion, can increase sound generation [1]. Studies have investigated such phenomena under the effect of blade design [2] as well as heat exchanger installation [3]. There have also been studies investigating the effect of inlet geometry [4] and more recently installation effect assessment from a free field operating fan to the final product integration [5].

However there have been only a few studies which have investigated these phenomena under the condition of parallel fan operation. Karlsson and Etemad [6] have studied a parallel multi-fan axial flow arrangement, investigating noise scaling effects, in the application area of automotive cooling fans. This study builds ups on the previous study, by investigating the spacing of the parallel fans along with the length of the inlet shroud. In addition acoustic measurements have been complemented with inlet flow velocity measurements performed by a Laser Doppler Anemometry (LDA) system.

2. MEASUREMENT SETUP

2.1 Measurement facility

All measurements (acoustic and aerodynamic) have been performed at the Fan Test Rig of VOLVO GTT. Fig. 1

*__Corresponding author__: michail.vourakis@chalmers.se.

showcases the layout of the facility. The closed loop, plenum to plenum fan performance facility, provides mass flow and temperature control while monitoring pressure and other thermodynamic properties. More information about the operation along with measurement accuracy of monitored parameters can be found in [7].

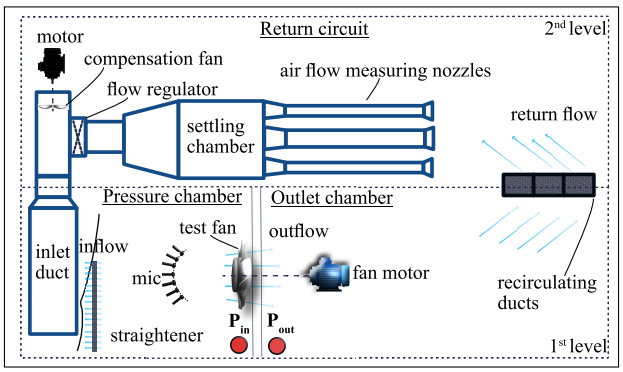

Figure 1. Schematic of Fan Test Rig.

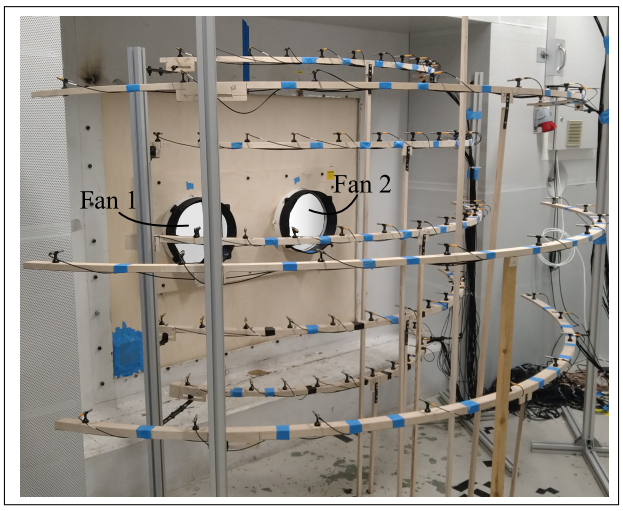

Figure 2. Acoustic measurement setup.

2.2 Acoustic measurements

Acoustic measurements were performed upstream of the fans at the pressure chamber. Fig. 2 gives an outlook of the acoustic measurement setup. The acoustic grid comprised of 101 quarter-inch free-field array microphones (type GRAS 40PH), centered around the geometric center of the two fans. 65 of the microphones were distanced at approximately 1 m radius while the remaining 36 at 1.5 m. Rotational speed of the fans was monitored via digital laser tachometers, while all signals were acquired via Simcenter SCADAS Mobile. Acquisition time was set to 30 s and sampling frequency at 51.2 kHz. Data processing was performed using MATLAB functions, linear spectra calculation via pwelch function while spectrogram was used for the short time Fourier transformations (both version R2019b). It should be noted here that the pressure chamber has a cut-off frequency of 200 Hz, thereby no acoustic spectra below that point will be shown in this analysis. More information about the acoustic setup can be found at [8].

The sound power level (SWL) of the fans was estimated by implementing [9]. Since the pressure chamber is not a hemi-anechoic room an environmental correction K_2 was calculated based on the two surface method. This calculation was performed for each setup case. Eqn. (1) gives the formula implemented for the calculation of SWL per 3^{rd} octave band in dB.

$$SWL = \overline{L_p} + 10log(\frac{S_1}{S_0}) - K_2 \quad (1)$$

Where $\overline{L_p}$, refers to the sound pressure average of all microphones at 1 m, S_1 to the half sphere surface of 1 m radius and S_0 to a reference surface of 1 m^2. The reference pressure level is 20 μPa. Inspection of the background noise in relation to the fan noise issued no need for background noise correction.

2.3 Aerodynamic measurements

Operating the Fan Test Rig at different volume flow settings allowed the acquisition of the characteristic curves for different fan setups. In addition velocity point measurements were performed upstream of one of the two parallel fans using a two component LDA probe, type 2D FiberFlow (Dantec Dynamics), in backscatter mode in line with BSA processor F600. The probe was placed sideways to the inlet duct (setup:x-z in Fig. 3), equipped with a lens of 400 mm focal length for acquiring the axial (x-direction) and the tangential/circumferential (z-direction) velocity component of the inlet flow. In addition, the LDA probe was equipped with a beam expander and a lens of 800 mm focal length and placed parallel to the axial direction of the inlet flow (setup:y-z in Fig. 3). That allowed acquisition of the radial (y-direction) and the tangential velocity component of the flow. Particle seeding was performed by the fog generator Viper NT (Look

Solutions USA), using glycol fluid (Look fluid regular-fog). Particle size is expected to be around 1 μm, according to the manufacturer.

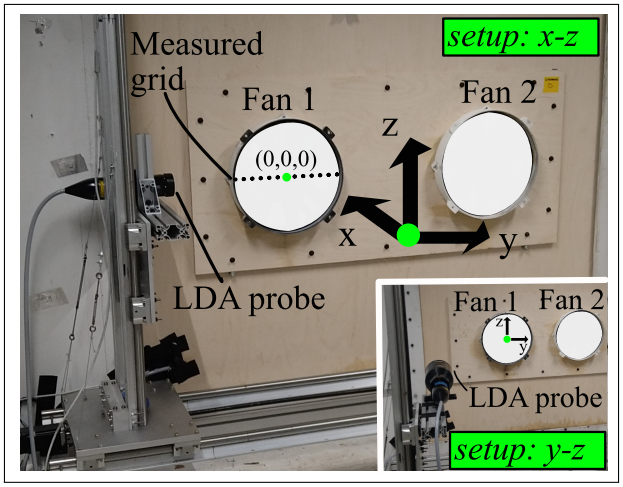

Figure 3. LDA setups for measuring axial (x), radial (y) and tangential (z) velocity components.

The measured grid comprised of 17 positions (where possible) across the radial direction. The line was located $\sim 0.13D$ upstream of the fan's aerodynamic interface. The stopping criteria for each acquisition was 90 s or 500000 samples. BSA Flow software (version 6.72) was used for data recording and monitoring. The measurement were performed in 'Burst' mode [10]. Mean velocity components were calculated by assuming a Gaussian normal distribution of acquired independent velocity samples. In addition transit time weighting was implemented for nullifying the velocity bias effect. The 95 % confidence limits of the mean velocity components in m/s, were estimated according to Eqn. (2).

$$c_i = \pm 1.96 \sqrt{\frac{\overline{U_i{}^2}}{N}} \tag{2}$$

Where $\overline{U_i{}^2}$ stands for the averaged square of each velocity component ($i : axial-x, radial-y, tangential-z$) and N for the number of samples. The frequency domain analysis of the velocity time series, was performed using the plomb MATLAB (version R2019b) function which implements the Lomb-Scargle method [11].

2.4 Fan and measurement cases

The fan used in this investigation is an axial cooling flow fan with a rotating ring. It comprises of seven non-equidistant blades with forward blade skew. The fan's diameter (D) is $\sim$ 0.3 m. The fan's detailed geometry is not disclosed, however it is employed for automotive cooling applications. Thereby the herein studies, focused on installation effects, treat the said fan as a sample case.

The fans were operated at a rotational speed of 4100 rpm. The spacing of the parallel fans was tested for three different cases, by utilizing different installation interfaces. Moreover two different inlet shrouds were tested. A cylindrical shroud of $\sim$ D/15 length (denoted as short) and one of $\sim$ D/4 length (denoted as long). Both shrouds had same constant diameter, while the rotating ring of the fan was not changed. These inlet shrouds were also used for the reference single fan measurement setup. Tab. 1 summarizes the acoustic measurement cases.

Table 1. Summary of acoustic measurement cases.

Fan spacing	**Shroud (length)**
0 (single fan)	long($D/4$),short($D/15$)
$1.25D$	long($D/4$),short($D/15$)
$1.5D$	long($D/4$),short($D/15$)
$2D$	long($D/4$),short($D/15$)

LDA measurements were performed for a few selected cases, included in Tab. 2. Where U_x,U_y and U_z stand for the axial, radial and tangential velocity component respectively. The measurement grid of the parallel fan cases for the axial component (see Fig. 3), was reduced due to lack of space for the traverse system. Measurements with the long shroud required the implementation of a glass interface due to the measured grid positions (i.e. downstream of long shroud's inlet). Unfortunately contamination of the glass interface prevented the acquisition of data that satisfied the set measurement criteria. Fig. 4 clarifies the location of the LDA measured grid in relation to the parallel fan cases.

Although different operating points were tested during the acoustic and LDA measurements, only one operating point will be presented in the following. That operating point represents the highest efficiency (for the tested rotational speed), which was calculated in relation to the fan's motor electric power consumption. Eqn. (3) showcases the formula used for the fan's efficiency calculation.

Table 2. Summary of LDA measurement cases.

Fan spacing - Shroud	Velocity component
0 (single fan) - short	U_x, U_y, U_z
$1.25D$ - short	reduced grid$(U_x), U_y, U_z$
$1.5D$ - short	reduced grid$(U_x), U_y, U_z$

$$n = \frac{\dot{V} dP_{ts}}{VI} \tag{3}$$

Where $\dot{V}$ is the volumetric flow rate in m^3/s and dP_{ts} is the total to static pressure difference in Pa, both averaged over a span of 30 s. V is the voltage ($Volt$) driving the fan's electric motor and I the corresponding current ($Ampere$). For the case of the parallel fans the electric power of both fans was summed.

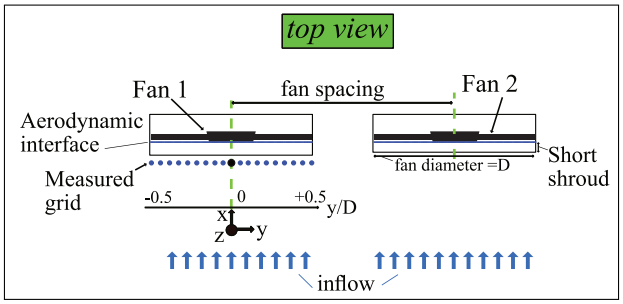

Figure 4. Sketch of LDA measurement cases for parallel fans.

3. RESULTS

3.1 Aerodynamics

Following the methods analysed in the previous section the characteristic curves of the parallel fan system are given. Fig. 5 shows the pressure rise over the volume flow for the different fan spacing. All curves are non-dimensional with respect to corresponding maximum pressure rise and volume flow. The top efficiency operating point is also marked. It can be observed that the effect of the spacing is minimal with the case of the the furthest spacing showing slightly worse performance at certain regions. Similar behavior is observed for the short inlet shrouds.

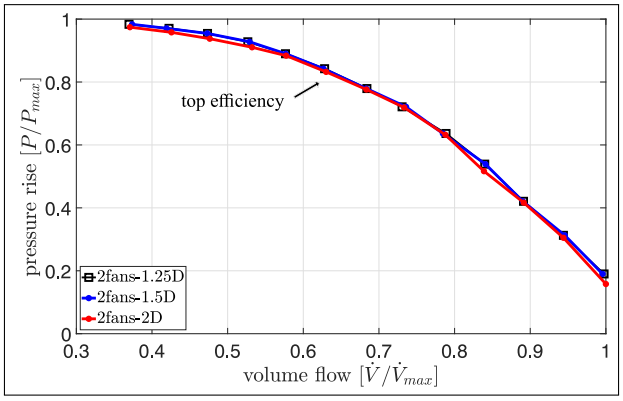

Figure 5. Characteristic curves of parallel fan system for different fan spacing and long inlet shrouds.

The effect of the shroud length is shown in Fig. 6. The higher pressure gain for the case of the long shroud is consistent throughout the single and parallel fan setups. In addition the employment of the longer shroud demonstrates a more stable behavior at the stall region of the curve. One should note the consistent scaling of the single fan system to the parallel fan system. That is the parallel fan system provides similar levels of pressure build-up for the double amount of volume flow.

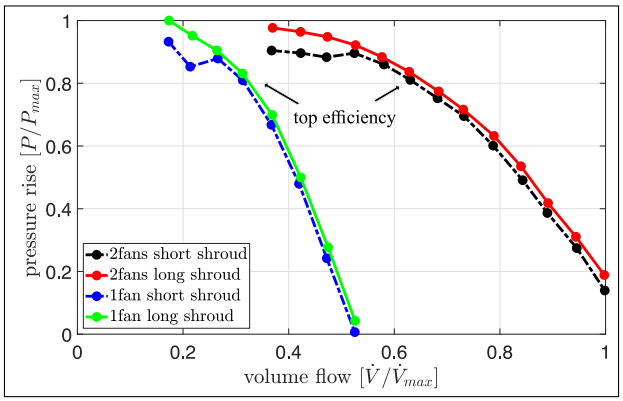

Figure 6. Characteristic curves of parallel fan system and single fan, for different shroud length.

The averaged velocity profiles upstream of Fan 1 (see Fig. 4) are given in the following. Velocity magnitudes and grid positions, are non-dimensional with regard to rotating ring speed ($V_{blade,y=0.5D}$) and fan diameter respectively. Fig. 7 showcases the axial velocity component for two different spacing of the parallel fan system. The cor-

responding profile for the case of the single fan is also included. Along the common grid points all cases have similar profile shape and differences are mainly captured towards positions which correspond to the radius of the fan's blade path closer to Fan 2 (see Fig. 4). It can also be noted that the parallel fan system with the furthest spacing is closer to the single fan profile. In an effort to investigate the sensitivity of the measured velocity profile to the neighbors fan inlet conditions, the rotational speed of Fan 1 (see Fig. 4) was kept constant while the rotational speed of Fan 2 was ranged within $\pm 2.5\%$. However same trends to Fig. 7 were observed for that rotational speed variation.

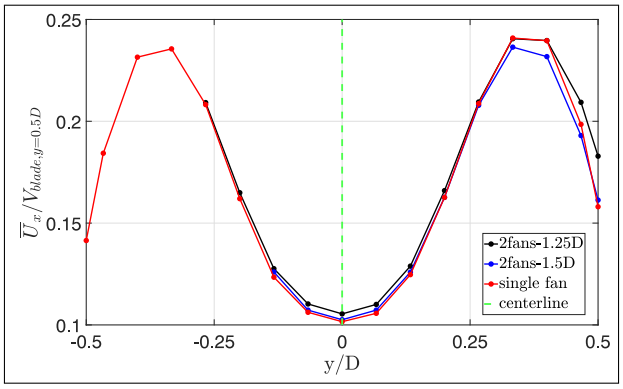

Figure 7. Axial direction velocity profile upstream of Fan 1 (short shroud).

The radial velocity component over the measurement grid is shown in Fig. 8. Firstly the symmetry of the single fan velocity profile is showcased, reaching the saddle point at the centerline. In comparison the parallel fan systems indicate a translation of the saddle point to the left. The parallel fan system with the further spacing (1.5 D) showcases values closer to the single fan case. Ranging of Fan's 2 rotational speed ($\pm 2.5\%$), while Fan's 1 rotational speed was kept constant, translated the saddle point of the radial velocity profile for either spacing. The effect was more prominent for the system with fans at 1.25 D.

The corresponding profile tangential velocity component is given in Fig. 9. Given the type of the fans and the location of the measurement grid, velocity magnitudes are lower compared to the other directions. Elaboration of consistent behavior based on the fan spacing is difficult to perform. There seems to be a reasonable agreement between the two measurement setups, with differences mainly attributed to alignment errors and selected measurement time.

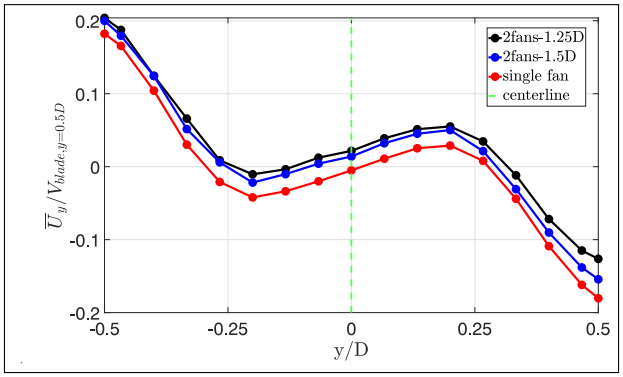

Figure 8. Radial direction velocity profile upstream of Fan 1 (short shroud).

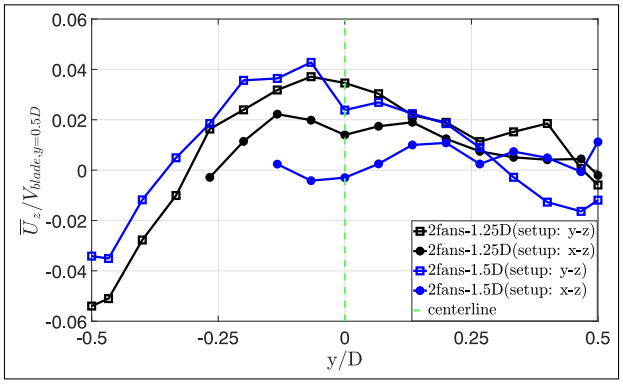

Figure 9. Tangential direction velocity profile upstream of Fan 1 (short shroud).

The analysis of the velocity components in the frequency domain produced similar results for the single and the parallel fan setup irrespective of the spacing and velocity component. Fig. 10 shows a representative power spectral density (psd) for two points along the measurement grid, one close to the center and one at the edge. The first motor order corresponds to the rotation frequency of the fan. Two main observations can be made. Firstly the upstream velocity components carry the information of the fundamental motor orders, including the blade passing frequency (bpf). Only the sixth motor order is not registered in the spectra calculated. Secondly moving towards the center of the measurement grid only the first and second motor order showcase important amplitudes values, while the higher orders drop significantly. Overall this character of standing out peaks at the motor orders, indicates that the majority of the energy is gathered there.

For the parallel fan system, ranging of Fan's 2 rotational speed ($\pm 2.5\%$),while Fan's 1 rotational speed was kept constant, did not provide any case where motor orders not corresponding to Fan 1 infiltrated into the calculated psd.

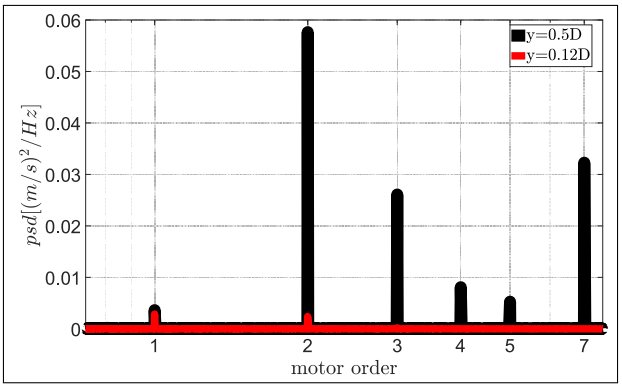

Figure 10. Power spectral density of U_x, at different radii.

3.2 Acoustics

Initially the acoustic character of the fan is studied by examining the acoustic spectra ($\overline{L_p}$ from Eqn. (1)). Fig. 11 summarizes the effect imposed by the fan spacing. Overall the fan spacing does not affect the character of the narrow band spectra. The magnitude differences observed, mainly at low motor orders, are attributed to the violation of the noise source's compactness, which is not taken into account when assessing the average sound pressure levels. The tonal characteristic of this particular fan is apparent, showcasing a dominant bpf. Contrary to the spectra of the velocity components (Fig. 10), significant contributions around motor order 6 in the acoustic spectra is evident. These contributions demonstrate broadband characteristics. Based on the characteristic of these contributions along with its relative position to the bpf, it could be linked to tip back flow vortices, which can be found in axial fans with rotating rings [12]. Similar results where observed for the long inlet shrouds, thereby the respective spectra are omitted.

Fig. 12 concerns the effect of the inlet shroud for a particular fan spacing. Overall the longer inlet shroud affects the acoustic spectra in two different ways. Firstly below motor order $\sim$ 20, which corresponds to a wavelength of $\sim$ 0.8D, spectra are amplified. This includes the broadband peak around motor order 6, which also showcases widening. Secondly beyond motor order $\sim$ 20, the

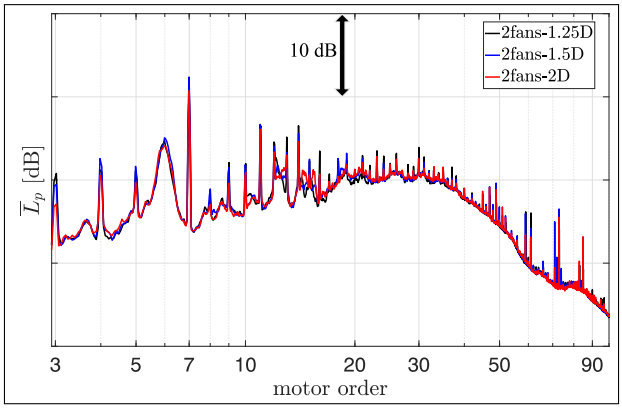

Figure 11. $\overline{L_p}$ of parallel fan systems for different spacing and short inlet shrouds.

spectra of the long shroud are attenuated. The extension of the shroud was introduced to improve the inlet velocity profile by guiding the flow in each fan without any interactions. However the general shift of the spectra hint towards an alteration of the system's radiation impedance, which possibly masks any inlet flow improvement.

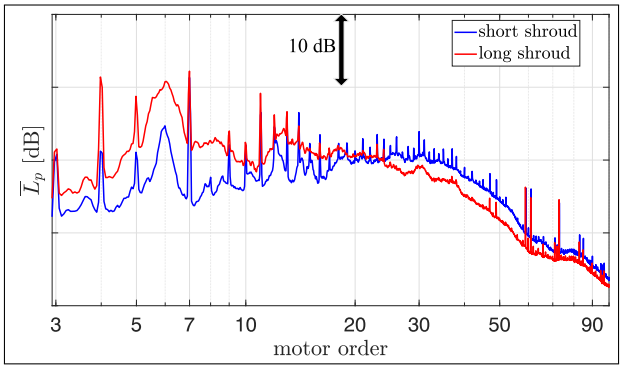

Figure 12. $\overline{L_p}$ of parallel fan systems for different inlet shroud length (spacing-1.25D).

Fig. 13 demonstrates the SWL (see Eqn. (1)) of the parallel fan systems for different spacing along with the single fan case. Since the effect of the acoustic environment is reduced, by employing the K_2 factor, the similar behavior of the parallel fan systems irrespective of fan spacing is clearer from a sound power perspective. Maximum differences are in the range of $\pm 1.2\ dB$. In addition one can observe the consistent scaling from the single fan to the parallel fan system, since the sound power

is overall doubled. Comparison of the SWL in relation to different inlet shroud length, carry the same information noted when examining Fig. 12. Lastly the same observations can be made about the behavior of the single fan.

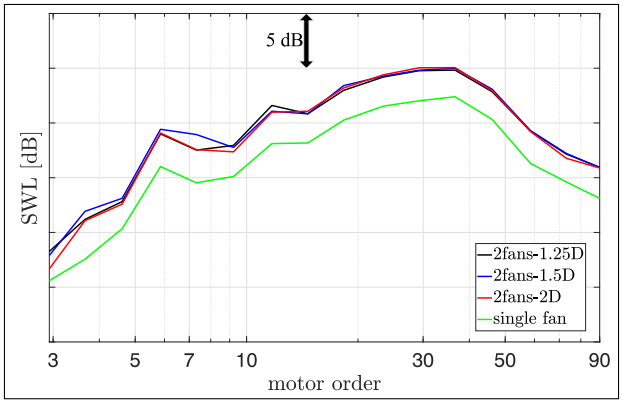

Figure 13. SWL of single fan and parallel fan systems for different spacing.

The effect of the inlet shroud length at the acoustic spectra for low frequencies (see Fig. 12), which carry the loudest tonal and broadband contributions, are highlighted on Fig. 14. The data presented concern recordings from the central microphone of the grid, 1 m from the geometric center of the parallel fan system. A representative case of a parallel fan system is chosen, since setups with different spacing gave similar results. Starting from the bpf (motor order 7), one can see the prominent sharpness of the short shroud case when compared to the longer shroud. Although the amplitude profile of the short shroud case indicates bigger changes over time, implying modulation effects, the authors of this study could not specify a strong case of "beating noise" from the recorded playbacks. A planned analysis based on tonality parameters [13], should indicate the importance of such discrepancies. In the same figure the spreading of the broadband character spectra, around motor order 6, is evident as well as its persistence with time. From a modulation character viewpoint, around the sixth order zone, the case of the long inlet shroud indicates more fluctuations over time, but this does not infer any periodicity.

4. DISCUSSION

A comprehensive experimental study on acoustic interference and flow interactions between parallel axial flow fans with rotating rings has been carried out. The focus was

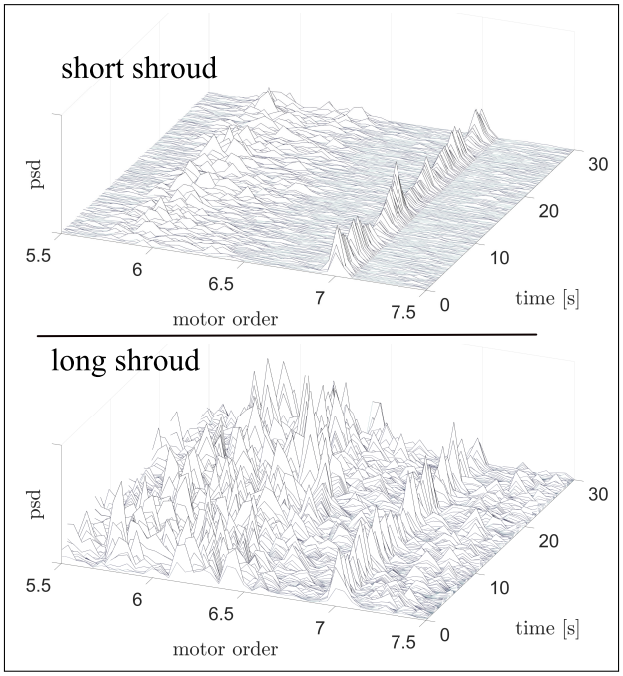

Figure 14. Power spectral density (psd), from parallel fan system with short (top) and long inlet shroud (bottom). Same psd scale used.

on inlet flow characterization via sound pressure and flow velocity measurements. The studied parameters were fan spacing and inlet shroud length.

The effect of the fan spacing, for the range analysed, proved to be minimal from an aerodynamic and acoustic performance perspective. Although the examination of upstream velocity profiles revealed an impact to its symmetry, when compared to the single fan case, the overall aerodynamic performance did not showcase any significant sensitivity when looking at the characteristic curves. Moreover the SWL analysis indicated minimal discrepancies while the character of the sound spectra, as perceived upstream of the fans, showcased stability and consistent scaling for the registered noise sources.

The longer inlet shroud provided a higher pressure gain while also extended the operational range of the parallel fan system. However the effects on the acoustic performance were mixed. The sound spectra of the fans with longer shrouds were significantly amplified up to frequencies that corresponded to wavelengths of $\sim 0.8D$. Within that range, peaks of broadband character were widened, which the short-time Fourier analysis further demon-

strated. Beyond the previous frequency range acoustic spectra were slightly attenuated.

The frequency domain decomposition of the velocity measurements, indicated a concentration of energy at the first motor orders, excluding the motor order before the first bpf. The former motor orders correspond to acoustic spectra of tonal character and the latter (excluded) motor order to acoustic spectra of broadband character. Moreover, the psd of the velocity components showcased spatial variation. Specifically the transition from hub to blade path radii corresponded to increased energy concentration at higher motor orders.

A currently ongoing tonality analysis, could further evaluate the acoustic perception effect issued by the highest amplitude tonal and broadband components. Moreover, considering the effect registered, in relation with the inlet length, responsible mechanisms are still under investigation. A complementary study where certain fan design parameters are isolated or an acoustically transparent inlet design is employed, may give further clarity.

5. ACKNOWLEDGMENTS

The authors of this study would like to acknowledge the valuable contribution of Associate Professor Sassan Etemad with regards to organizing and undertaking of the measurements at the Fan Test Rig of VOLVO GTT. In addition Dr. Randi Franzke is acknowledged for setting up the velocity measurement equipment and provision of technical support during the measurements.

6. REFERENCES

[1] W. Neise, "Review of fan noise generation mechanisms and control methods," in *Proc. of the International Symp. on Fan Noise*, (Senlis, France), pp. 45–56, 1992.

[2] F. J. Zenger, A. Renz, M. Becher, and S. Becker, "Experimental investigation of the noise emission of axial fans under distorted inflow conditions," *Journal of Sound and Vibration*, vol. 383, pp. 124–145, 2016.

[3] F. Czwielong, F. Krömer, and S. Becker, "Experimental investigations of the sound emission of axial fans under the influence of suction-side heat exchangers," in *Proc. 25th AIAA/CEAS Aeroacoustics Conference*, (Delft, The Netherlands), 2019.

[4] T. Benedek, J. Vad, and B. Lendvai, "Combined acoustic and aerodynamic investigation of the effect of inlet geometry on tip leakage flow noise of free-inlet free-exhaust low-speed axial flow fans," *Applied Acoustics*, vol. 187, p. 108488, 2022.

[5] Y. Lai, C. Weng, Y.-Y. Lu, M. Karlsson, M. Abom, and M. Knutsson, "Study of installation effects on automotive cooling fan noise," in *Proc. 12th International Styrian Noise, Vibration and Harshness Congress: The European Automotive Noise Conference*, (Graz , Austria), pp. 803–809, 2022.

[6] M. Karlsson and S. Etemad, "Installation effects on the flow generated noise from automotive electrical cooling fans," in *Proc. 11th International Styrian Noise, Vibration and Harshness Congress: The European Automotive Noise Conference*, (Graz , Austria), 2020.

[7] P. V. Gullberg, *Optimisation of the Flow Process in Engine Bays - 3D Modelling of Cooling Airflow*. PhD thesis, Gothenburg, Sweden,: Chalmers University of Technology, 2011.

[8] M. Vourakis and M. Karlsson, "A round robin test of a low-pressure axial fan," in *Proc. FAN 2022-International Conference on Fan Noise, Aerodynamics, Applications and Systems*, (Senlis, France), 2022.

[9] *ISO 3744:2010 Acoustics — Determination of sound power levels and sound energy levels of noise sources using sound pressure — Engineering methods for an essentially free field over a reflecting plane*. International Organization for Standardization, 2010.

[10] *BSA flow software user guide*. Dantec Dynamics, 2019.

[11] J. H. Horne and S. L. Baliunas, "A prescription for period analysis of unevenly sampled time series," *The Astrophysical Journal*, vol. 302, pp. 757–763, 1986.

[12] S. Magne, S. Moreau, and A. Berry, "Subharmonic tonal noise from backflow vortices radiated by a low-speed ring fan in uniform inlet flow," *The Journal of the Acoustical Society of America*, vol. 137, no. 1, pp. 228–237, 2015.

[13] W. R. Bray, "A new psychoacoustic method for reliable measurement of tonalities according to perception," in *Proc. InterNoise18, Aerodynamics, Applications and Systems*, (Chicago,Illinois), pp. 440–450, 2018.